Journal of Nuclear Materials 527 (2019) 151797

Contents lists available at ScienceDirect

Journal of Nuclear Materials

journal homepage: www.elsevier.com/locate/jnucmat

An exploration of measuring lower-length-scale structures in nuclear materials: Thermal conductivity of U-Mo fuel particle

Yinbin Miao [a, *], Manjunath C. Rajagopal [b], Krishna Valavala [b], Kun Mo [a], Zhi-Gang Mei [a], Sumit Bhattacharya [a], Laura Jamison [a], Sanjiv Sinha [b, c], Abdellatif M. Yacout [a]

[a] Chemcial & Fuel Cycle Technologies Division, Argonne National Laboratory, Argonne, IL, 60439, United States
[b] Department of Mechanical Science & Engineering, University of Illinois, Urbana, IL, 61801, United States
[c] Micro and Nanotechnology Laboratory, University of Illinois, Urbana, IL, 61801, United States

ARTICLE INFO

Article history:
Received 20 May 2019
Received in revised form
5 September 2019
Accepted 10 September 2019
Available online 13 September 2019

Keywords:
Dispersion fuel
Thermal conductivity
Nanotechnology
Microstructure characterization

ABSTRACT

The feasibility of utilizing the suspended bridge method, which was originally developed for one-dimensional or nearly-one-dimensional nanomaterials, to measure the thermal conductivity of lower-length-scale structures in nuclear materials is explored in this study. Nanoribbon specimens of stainless steel SS304, representing materials with well-known thermal conductivity, and atomized U-Mo alloy particles used in dispersion fuels for research reactors, representing new nuclear materials with limited thermal conductivity data reported, were made using focused ion beam (FIB). The contact thermal resistance was corrected by measuring a series of specimens with different bridge lengths. The measured thermal conductivity of SS304 was found to be consistent with that reported for bulk samples. The thermal conductivity of U-Mo particles measured using the suspended bridge method was also analyzed and compared with literature data of monolithic U-Mo alloys. *Ab initio* molecular dynamics (AIMD) was used to quantitatively demonstrate that the reduced specimen size only has marginal effects on the measured thermal conductivity compared to the bulk specimens. The novel concept of utilizing the suspended bridge method in nuclear material research is proven and future work is discussed.

1. Introduction

As an essential part of the world energy portfolio, the development of advanced nuclear energy technologies that feature enhanced safety and efficiency is important to a sustainable world economy. Nowadays, extending the understanding of conventional nuclear materials to better predict and improve the performance of the current nuclear fleet and searching for innovative nuclear materials for next-generation nuclear systems are becoming major challenges in advancing nuclear technologies [1]. As a thermal power system, the thermophysical properties of the materials used in a nuclear reactor are crucial to both the efficiency and safety [2]. Therefore, in order to increase the economical profitability and accident tolerance of nuclear energy, it is of great significance to accurately measure and/or reliably predict the thermophysical properties, thermal conductivity in particular, of materials used in nuclear systems.

However, in nuclear reactors, materials experience extreme environmental conditions, including elevated temperature, high pressure, aggressive corrosion, and intense radiation. In advanced nuclear reactor concepts, the operation conditions are usually even tougher than current commercial light water reactors (LWRs) [3]. Under such conditions, nuclear materials are subject to a series of microstructural modifications, such as cavity nucleation/growth, oxidation, secondary phase precipitation, grain growth/subdivision and interface reaction. These microstructural changes degrade the material performance, including thermophysical properties. Establishing a comprehensive correlation between the microstructural modifications and their contributions to thermophysical properties is key to the reliable prediction of the shifts in material properties and consequent degradation in performance.

Traditional measurement techniques for thermal conductivity are unable to differentiate the impact of the microstructural changes on the length scale of interest. Meanwhile, with the development of material science and fabrication technologies, nuclear materials with intrinsic lower-length-scale (LLS) structures

* Corresponding author.
E-mail address: ymiao@anl.gov (Y. Miao).

https://doi.org/10.1016/j.jnucmat.2019.151797
0022-3115/

have been developed to provide enhanced materials properties. For instance, Sub-millimeter TRISO particle, which is developed for high-temperature gas-cooled reactors, has its own multi-layered fuel-buffer-cladding system [4]; dispersion fuel consisting of Al matrix and U-Mo micro-particles is the promising candidate fuel to enable the conversion of European high-power research reactors from using high-enriched uranium (HEU) to low-enriched uranium (LEU) [5–8]; Nickel superalloys featuring dense sub-micron γ' intermetallic precipitates are considered as candidate structural materials for a series of advanced reactor concepts that involve high operating temperatures that exceed stainless steels' capability [9]. Knowledge about these microstructural features and their contributions to thermophysical properties is also essential for the evaluation and qualification of these new material concepts.

As one of the most important thermophysical properties, thermal conductivity determines the maximum temperature and the efficiency of heat transfer of a nuclear reactor. However, conventional thermal conductivity measurement techniques, such as the laser flash method [10], are developed to measure macroscopic specimens (millimeter or beyond). Therefore, directly measuring thermal conductivity of LLS structures had been an impossible mission until the dawn of this millennium. The rapid development of nanomaterials has inspired the innovation of a series of revolutionary measurement methods that are designated for micro- and nano-scale specimens. Several pioneering efforts have been made to apply one of these innovative methods, thermal reflectance, to measure nuclear materials with reduced dimension [11–13]. However, because the thermal reflectance based methods have been developed to measure local thermal conductivity in either bulk materials or thin films, such techniques can hardly handle other lower-length-scale structures such as thin nanorods. Therefore, techniques other than thermal reflectance must be explored so that a comprehensive capabilities of thermophysical properties measurement can be established for the nuclear material community. A microfabricated device termed suspended bridge was developed to measure thermal conductivity of one-dimensional nanomaterials [14,15]. The aforementioned device was based on a one-dimensional nanomaterial specimen bridging a heating membrane and a sensing membrane and used fundamental one-dimensional heat conduction principles to measure the thermal conductivity of the bridging material. This technique has been successfully applied to measure thermal conductivity of a series of nanomaterials including carbon nanotubes [14], Si nanowires [16], and SnO_2 nanobelts [17].

The major challenge of using the microfabrication-based technique to measure the thermal conductivity of the LLS features in nuclear materials is to separate the microstructures of interest with precise control of the sampling position and specimen dimension. Fortunately, contemporary focused ion beam (FIB) techniques have enabled microfabricating miniature specimens of LLS structures with satisfactory precision. In this study, the feasibility of thermal conductivity measurement of LLS structures in nuclear materials was explored by combining the state-of-the-art nanoscale measurement method and the advanced FIB microfabrication technique. The innovative technique was first validated by measuring the thermal conductivity of a well-studied material (SS304). Then, the thermal conductivity of a U-Mo fuel particle was measured to demonstrate the great impact of this technique.

2. Experiments

2.1. Suspended bridge method

The suspended bridge method was originally developed by Shi et al. [15] and was also used by Ghossoub et al. [18] to measure the thermal conductivity of silicon nanowires. In general, this method is capable of measuring the thermal conductivity of one-dimensional or nearly-one-dimensional nanomaterials such as nanotubes, nanowires and nanobelts. In Sections 2.1 through 2.3, the measurement technique and the art of sample preparation are briefly described to readers previously unaware of the suspended bridge method. The fundamental principle of this technique is illustrated in Fig. 1 (a). Two membrane platforms made of thermally and electrically insulating materials such as silicon nitride (SiN_x) are suspended and supported by six thin beams. On each suspended platform, platinum lines are patterned to form an electrical resistor. The platinum resistor is connected by four other platinum probes through four of the six supporting beams. A nanoribbon specimen can be mounted to bridge the two platforms. The rest of the four beams supporting the two platforms also have platinum electrodes so that the electrical resistance of the nanoribbon can be measured using the four-probe method (not used in this study).

The measurement is done under vacuum ($\sim 10^{-6}$ Torr) in a cryostat to minimize convective heat loss. The ambient temperature can be controlled between liquid nitrogen temperature ($\sim$80 K) and 400 K, where the contribution from thermal radiation is negligible. A DC heating current is applied to the resistor circuit of one platform (termed the heating platform). As a result, the heating power on the platinum resistor is Q_h, and the heating power on each of the two beams through which the current flows is Q_L. The generated heat can either go to the environment through the six beams supporting the heating platform (marked as Q_1), or can flow to the other platform, which is termed the sensing platform, through the bridge specimen and then flows to the environment through the six beams supporting the sensing platform (marked as Q_2). The temperatures of the heating and sensing platforms are T_h and T_s, respectively. The temperature difference between the two platforms is kept under 6 K by limiting Q_L and Q_h. Assuming the total thermal conductance of the six beams of each platform and the bridge specimen to be G_b and G_{bs}, respectively, (i.e. each beam's thermal conductance is $G_b/6$), the following equations can be used under steady-state conditions (detailed derivation can be found in the Supplementary Material):

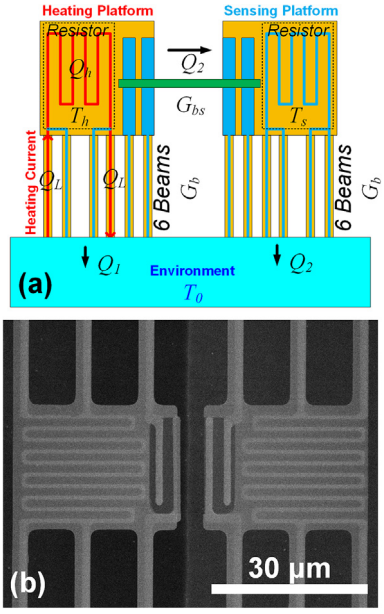

Fig. 1. The fundamental principle of the thermal conductivity measurement: (a) a schematic showing the measurement circuit; (b) a SEM image of an actual microfabricated measurement device (the bridge specimen is not mounted).

$$G_b = \frac{Q_h + Q_L}{(T_h - T_0) + (T_s - T_0)}; \quad (1)$$

$$G_{bs} = G_b \frac{T_s - T_0}{T_h - T_s}. \quad (2)$$

The thermal conductance of the measured specimen (G_{bs}), which is the reciprocal of the thermal resistance (R_{bs}), can be used to deduce the thermal conductivity of the sample. Details of this calculation will be provided in Section 2.4.

2.2. Micro-fabrication of measurement devices

The heating and sensing platforms were batch fabricated from a 4" double-side polished (DSP) Si wafer with a thickness of 300 μm. The Si wafer is p-doped (10∼20 Ω•cm). Stress-free SiN_x (300 nm) was deposited using plasma-enhanced chemical vapor deposition (PECVD) using an STS Multiplex PECVD operated at a mixture of 13.56 MHz and 380 kHz. 3/30 nm Ti/Pt metal film was evaporation deposited using a CHA E-beam metal evaporator. This metal film was coated with a 70 nm PECVD silicon nitride. Using photolithograph (EVG 620 mask aligner), photoresist (PR) AZ 5214 was patterned to the shape of the platinum resistors. The exposed SiN_x was removed by Freon reactive ion etching (RIE). After removing the remaining PR, the patterned SiN_x was used as an etch mask to remove the exposed platinum through argon plasma in a Plasma-Therm ICP-RIE (inductively coupled plasma reactive ion etching) device. Photolithography and Freon RIE were used to pattern the SiN_x platforms, and also to expose the platinum at contact pads. The platforms were suspended through a bulk-Si etching in 45% aquatic KOH solution at 70°C. More details on the fabrication of suspended platforms can be found in Ref. [18].

2.3. Sample preparation

In this study, two types of materials were investigated: stainless steel SS304 (Fe-18Cr-8Ni) in the form of bulk bars and micro-scale U-Mo alloy in the form of particles. The SS304 investigated in this study is an as-received alloy bar procured from McMaster-Carr. The U-Mo alloy examined in this study are particles with approximately 50 μm diameters. The U-Mo particles were prepared in KAERI (Korea Atomic Energy Research Institute) through atomizing the molten alloy in a helium atmosphere and have a nominal composition of U-7Mo (weight percentage). The as-atomized particles were further annealed at 1000°C for 1 h to increase the grain size and improve homogeneity. The annealed U-Mo powder is primarily γ phase with a limited amount of residual α and γ' phases. Only a single atomized U-Mo particle was used to prepare all the specimens measured in this study.

Both SS304 and annealed U-Mo particles have relatively large grain size ($> 10\ \mu m$). During sample preparation, all the investigated specimens of each material were intentionally prepared from one single grain. The inclusion phases (i.e. carbides and residual α/γ' phases), which have limited volume fractions, were averted during sample preparation to ensure that the specimens prepared from each material have similar microstructure. In SS304 matrix, the distribution of Fe, Cr and Ni is uniform. For atomized U-Mo particles, annealing at 1000°C helps homogenize Mo concentration within each particles [19]. The homogeneous distribution of elements in the SS304 and U-Mo particles investigated in this study was confirmed by energy dispersive X-ray spectroscopy (EDS), as shown in Fig. 2.

The sample preparation was performed using a FEI Strata 400 focused ion beam (FIB) system. A 20 μm × 10 μm × 1 μm thin foil sample was first milled and lifted out from the bulk sample and mounted on an Omniprobe TEM sample grid, which is similar to the standard FIB TEM sample preparation procedure (see Fig. 3(a)). The foil was then further thinned to ∼300 nm in thickness. The entire TEM sample grid was then tilted by 90° so that the FIB could work vertically on the cross section. As shown in Fig. 3(b), a thin rod with a rectangular cross section can be fabricated. The rod can then be cut off and transferred to the measurement platform using a tungsten Omniprobe tip (see Fig. 3(c)). The rod sample was adhered to the heating and sensing membranes of the measurement device using platinum (Pt) deposition available in the FIB to minimize the contact thermal resistance (Fig. 3(d)). In order to correct for the contact thermal resistance, for each material, multiple rod specimens with different lengths ranging from approximately 3 μm−20 μm were prepared. The different lengths were achieved by mounting the thin rod specimens onto platforms at different angles. The detailed dimensions of all the investigated samples are provided with the corresponding measurement uncertainties in the Supplementary Material. The detailed method for accounting for thermal contact resistance will be described in Section 2.4.

2.4. Measurement and data analysis

The measured thermal resistance ($R_{bs} = G_{bs}^{-1}$) of the specimen consists of at least three components: the "bridge" part of the sample (R_{bridge}) and the two contacts at the heating and sensing islands ($R_{contact,h}$ and $R_{contact,s}$). That is,

$$R_{bs} = R_{bridge} + R_{contact,h} + R_{contact,s}. \quad (3)$$

As shown in Fig. 4(a), the "bridge" part of the sample, which has

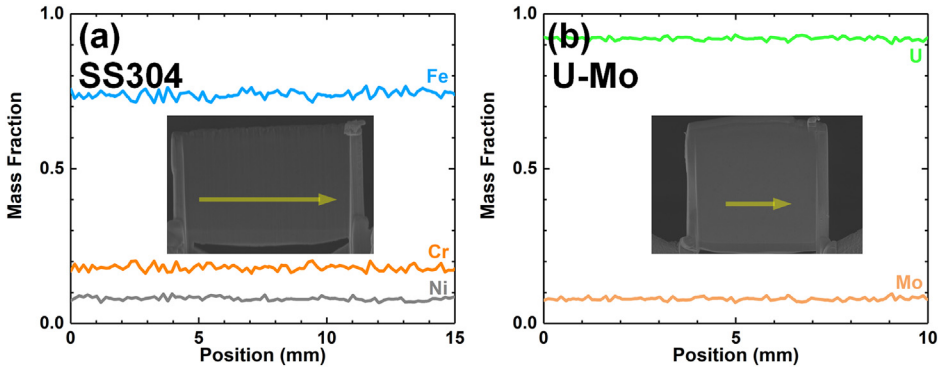

Fig. 2. SEM EDS data showing the homogeneity in composition of SS304 and U-Mo. Note that the EDS was not performed on the same lift-out slices that were used for thermal conductivity measurement to prevent surface modification caused by long-duration focused electron beam. (a) SS304; (b) U-Mo.

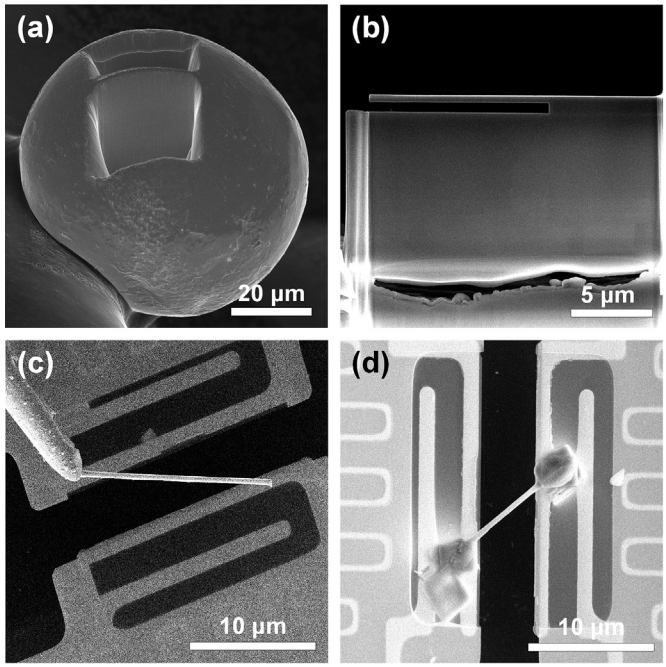

Fig. 3. The art of sample preparation: (a) a thin foil milled from an atomized and heat treated U-Mo fuel particle; (b) a lift-out thin foil mounted on an Omniprobe TEM sample grid with a thin rod prepared; (c) a cut-off thin rod specimen being transferred to the measurement platform using a tungsten Omniproble tip; (d) a thin rod specimen mounted on the measurement platform using Pt deposition.

a length of L, width of w, and a depth of d, is solely made of the material to be investigated. On the other hand, the contact lengths are L_h and L_s, respectively. All the three lengths (i.e. L, L_h, and L_s) were measured from the middle of the d direction so that the contact areas can be calculated using the product of $L_{h/s}$ and d regardless to the mounting angle, as illustrated by Fig. 4(b).

Assuming one-dimensional heat conduction, the thermal resistance of the bridge part has the expression as follows:

$$R_{bridge} = \frac{L}{kwd}, \tag{4}$$

where, k is the thermal conductivity of the material of interest. For the two contact resistance components, it was assumed that the resistance is inversely proportional to the contact area:

$$\begin{aligned} R_{contact,h} &= \frac{C}{L_h d}, \\ R_{contact,s} &= \frac{C}{L_s d}, \end{aligned} \tag{5}$$

where C is a constant. Thus, Equation (3) becomes:

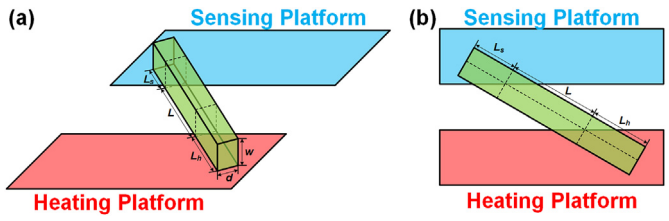

Fig. 4. A schematic showing the physical quantities involved in the thermal conductivity measurement and contact resistance correction: (a) pictorial drawing; (b) top view.

$$R_{bs} = \frac{L}{kwd} + \frac{C}{L_h d} + \frac{C}{L_s d}. \tag{6}$$

Let $L_{contact}$ be half of the harmonic mean of L_h and L_s, namely, $L_{contact} = L_h L_s/(L_h + L_s)$. Equation (6) can then be written in the following form,

$$R_{bs} d L_{contact} = \frac{L L_{contact}}{w}\frac{1}{k} + C. \tag{7}$$

Thus, by measuring a series of specimens with different dimensions, the thermal conductivity of the materials of interest can be deduced using linear regression.

3. Results

Using the measurement technique and analysis method described above, SS304, a widely-used material with well-understood properties, was first investigated to validate the feasibility of applying this novel thermal conductivity measurement method originally developed for one-dimensional nanomaterials to other classes of materials. Six SS304 thin rod specimens with different lengths were prepared and measured. The thermal conductivity was measured at multiple temperatures ranging from 300K to 400K. The linear regression for the contact thermal resistance correction at 300 K can be found in Fig. 5(a). The linearity of the data looks prominent (R^2 is higher than ~0.9), demonstrating that the data analysis model described above is appropriate. A similar approach was also used for a U-Mo fuel particle. Seven thin rod specimens were prepared and investigated. The thermal conductance results of U-Mo measured at 300 K and corresponding linear fitting are shown in Fig. 5(b). At other measurement temperatures, the behavior of those SS304 and U-Mo specimens is similar to that shown in Fig. 5(a) and (b). Consequently, the thermal contact resistance correction method used in this study yields reasonable results for both SS304 and U-Mo between 300 K and 400 K. The uncertainty of this thermal conductivity measurement technique stems from (a) the thermal resistance measurement, (b) the dimension measurement, and (c) the linear regression. The uncertainties in thermal resistance measurement (~10^5 K/W) are typically an order of magnitude lower than measured thermal resistance, while the dimension measurement uncertainties are approximately two orders of magnitude lower than the measured values. Therefore, the reported uncertainties in thermal conductivity predominantly arise from the fitting uncertainties of Equation (7). Physically, the fitting error arises from the fact that the contact resistance of unit area (C) may not be uniform across multiple samples. The detailed values of measurement uncertainties and their propagation can be found in the Supplementary Material.

According to the intercepts in Fig. 5(a) and (b), at 300 K, the SS304 specimen and the platform bonded by platinum has a contact resistivity of 4.77×10^{-6} K·m^2/W, while the U-Mo rod and the platform has a contact resistivity of 6.30×10^{-6} K·m^2/W. The values are comparable and the difference can be attributed to material-specific properties. The slopes of the lines in Fig. 5(a) and (b) are the thermal resistivity values of SS304 and U-Mo at 300 K, which are 7.36×10^{-2} K·m/W and 10.11×10^{-2} K·m/W, respectively. Therefore, the thermal conductivity of SS304 and U-Mo at 300 K, which is the reciprocal thermal resistivity, can be deduced to be 13.58 W/mK and 9.894 W/mK, respectively.

The linear regression based contact resistance correction gives material dependent contact resistivity on the order of 10^{-6} K·m^2/W. This magnitude yields a contact thermal resistance that is comparable to the thermal resistance of the measured specimens themselves. For instance, at 300 K, for U-Mo specimens with

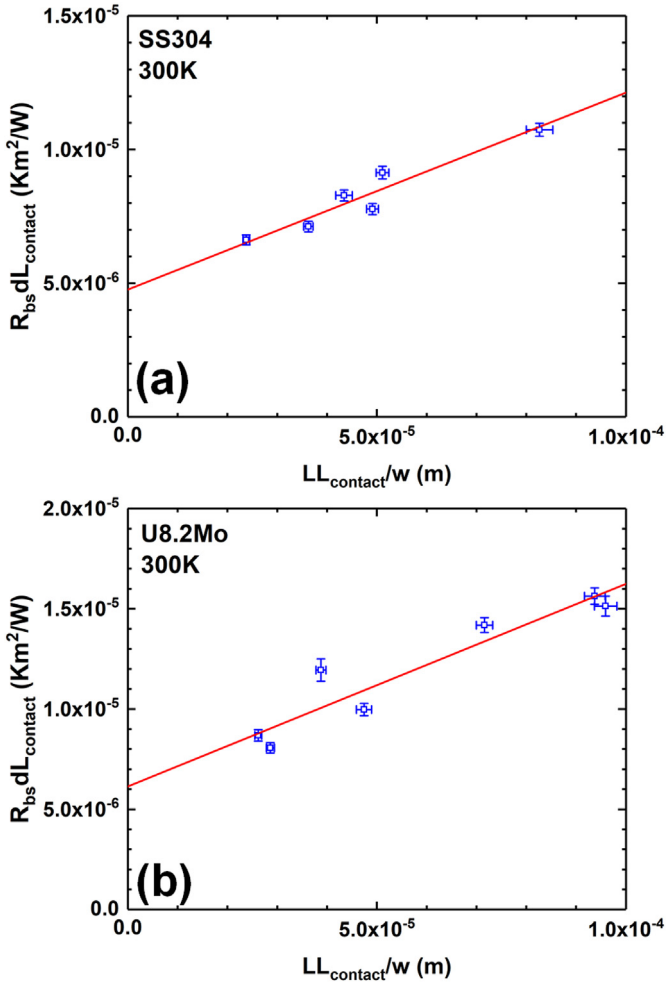

Fig. 5. Measurement results and corresponding contact resistance correction: (a) measurement and correction results of the six SS304 specimens at 300 K; (b) measurement and correction results of the seven U-Mo specimens at 300 K.

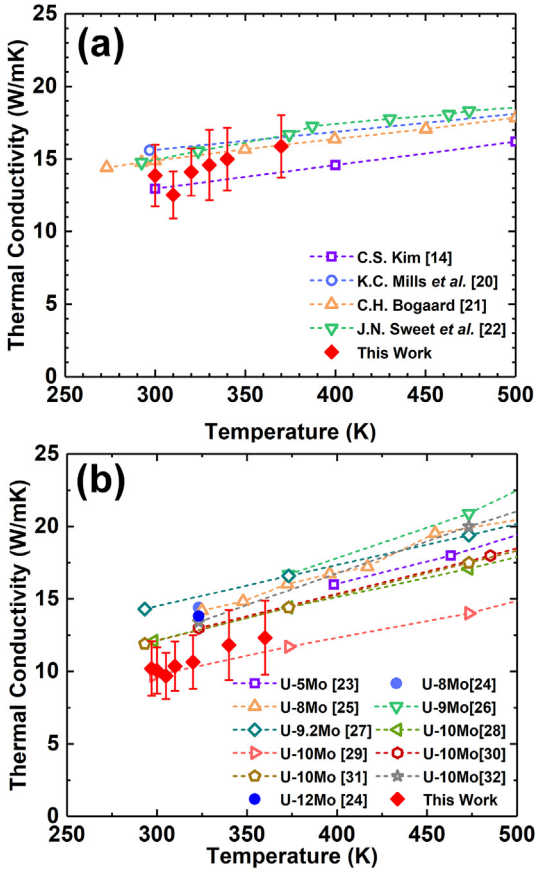

Fig. 6. Measured thermal conductivity in comparison with related literature data: (a) measured thermal conductivity of SS304 compared to a series of reported SS304 data [14,20–22]; (b) measured thermal conductivity of the nominal U-Mo particle compared to the data of various U-Mo alloys (U-5Mo [23], U-8Mo [24,25], U-9Mo [26], U-9.2Mo [27], U-10Mo [28–32] and U-12Mo [24]).

various lengths, the thermal resistance of the specimens themselves ranges from 2.7×10^6 K/W to 1.4×10^7 K/W while the thermal contact resistance is between 5.5×10^6 K/W and 1.0×10^7 K/W. Obviously, the thermal contact resistance between the specimen and the heating and sensing platforms makes a considerable contribution to the measured resistance value, which cannot be neglected. Therefore, the correction of contact resistance is essential to obtain accurate thermal conductivity of the materials of interest. The linearity of data (as shown in Fig. 5(a) and (b)) indicates that Eq. (7) can be employed to extract the value of the thermal contact resistances with acceptable reliability.

The temperature-dependent thermal conductivity of SS304 and U-Mo can be derived based on the measurement results collected at temperatures ranging from 300 K to 400 K, as shown in Fig. 6. The thermal conductivity of both materials increases with temperature. The thermal conductivity of SS304 [14,20–22] and U-Mo alloys [23–32] reported in literature are also provided in Fig. 6 for comparison to the measured values in this study. The measured data are within the range of reported values of the same class of materials.

3.1. Theoretical analysis of the reduced-size effect

One of the major concerns of applying the suspended bridge method to nuclear material research is the effect of the reduced specimen size. In alloy materials such as SS304 and U-Mo investigated in this study, the thermal conductivity has two components, lattice thermal conductivity contributed by lattice wave (i.e. phonons) and electronic thermal conductivity contributed by free electrons. The reduced size of a specimen only significantly affects the thermal conductivity measurement when the specimen dimension is comparable to or lower than the mean free path of carriers. In elemental metals, the mean free path of free electrons, which dominate the thermal conductivity, is on the order of tens of nanometers [33]. In alloys, however, alloying elements scatter free electrons, considerably reducing the mean free path to nanometer, or even subnanometer level, degrading electronic thermal conductivity. Therefore, the ~300 nm cross section dimension of the specimens investigated here is several orders of magnitude higher than the mean free path of free electrons, making the size effect negligible. However, in alloy materials, the mean free path of the phonons (the contributor to the lattice thermal conductivity) may be as high as ~100 nm, which requires further detailed investigations to determine the impact of sample size.

Theoretically, the lattice thermal conductivity ($\kappa_{\alpha\alpha}$) of a material can be calculated as:

$$\kappa_{\alpha\alpha} = \frac{1}{V}\Sigma_{\mathbf{qs}} C_{\mathbf{qs}} v^2_{\alpha\mathbf{qs}} \tau_{\alpha\mathbf{qs}}, \tag{8}$$

where V is the crystal volume, $C_{\mathbf{qs}} = \hbar\omega_{\mathbf{qs}}\partial n^0_{\mathbf{qs}}/\partial T$ is the mode specific heat, $v_{\alpha\mathbf{qs}}$ is the phonon velocity in mode $\mathbf{qs}$, and $\tau_{\alpha\mathbf{qs}}$ is the

phonon lifetime for transport in that direction. The phonon lifetime can be determined from a full iterative solution of the phonon Boltzmann transport equation (BTE) [34,35] with accurate descriptions of the harmonic and anharmonic interatomic force constants in a material. The temperature-dependent effective potential (TDEP) method [34,36,37] was adopted to calculate the second- and third-order interatomic force constants (IFCs), which can be determined from *ab initio* molecular dynamics (AIMD) trajectories and forces. For the AIMD simulations, 256-atom (192 Fe, 16 Ni, 48 Cr) and 128-atom (104 U, 24 Mo) supercells were used for SS304 and U-Mo alloy systems, respectively. Only Γ-point was used for the Brillouin zone integration combined with a cut-off plane-wave energy of 400 eV. AIMD simulations were run at 300 K in canonical ensemble. Temperature was controlled using a Nosé thermostat. The simulations ran for 12 ps with a time step of 2 fs. All the AIMD calculations were performed using the projector augmented wave method (PAW) [38] as implemented in the Vienna ab initio simulation package (VASP) [39,40], and the electronic exchange-correlation potential was described by the generalized gradient approximation (GGA) parameterized by Perdew-Burke-Ernzerhof (PBE) [41]. In the SS304 and U-Mo alloy systems, phonon transport is subjected to scattering due to lattice disordering, which are considered as isotope scattering on the phonon life time. At 300K, the lattice thermal conductivities of SS304 and U-Mo were predicted to be 7.61 W/mK and 1.66 W/mK, respectively. The calculated cumulative lattice thermal conductivity, which is the thermal conductivity contributed by the phonons with mean free paths lower than a given value, indicates that phonons with mean free path less than 100 nm contribute about 95% and 87% of the total lattice thermal conductivity in the bulk SS304 and U-Mo, respectively. For constrained geometries, e.g., thin rods in this case, the phonon transport will be subjected to additional scattering from domain boundaries. Fig. 7(a) shows the calculated lattice thermal conductivities of SS304 and U-Mo alloys as a function of domain size. Consistent with the calculated cumulative lattice thermal conductivity, the lattice thermal conductivities of SS304 and U-Mo are only notably affected when the sample dimension is reduced to less than 100 nm (this is prominent after normalization as shown in Fig. 7(b)). Therefore, the size of the nanorods used for the thermal conductivity measurement in this work should have a minimal impact on the lattice thermal conductivity as compared to their bulk phases.

Consequently, for both materials investigated in this study (and other alloy materials), the reduced dimension involved in the suspended bridge only marginally affects the measured thermal conductivity. In summary, the overall impact of the size effect is marginal for alloy materials (e.g., stainless steels and U-Mo), which account for the majority of the nuclear materials. Additionally, many radiation-induced microstructural features intrinsically have a limited dimension in nuclear materials. Adopting the technique introduced in this study may involve miniature specimens with the reduced dimension that is similar to the intrinsic dimension of the radiation-induced microstructural features and therefore provide more reliable measurement results compared to bulk measurement methods.

4. Discussion

4.1. Consistency with conventional measurement

As indicated in Fig. 6, the thermal conductivity measured by this method is within the range of reported values available in literature. However, some of the measured values are slightly lower than the thermal conductivity of the same class of materials measured by conventional methods. In particular, the measured thermal

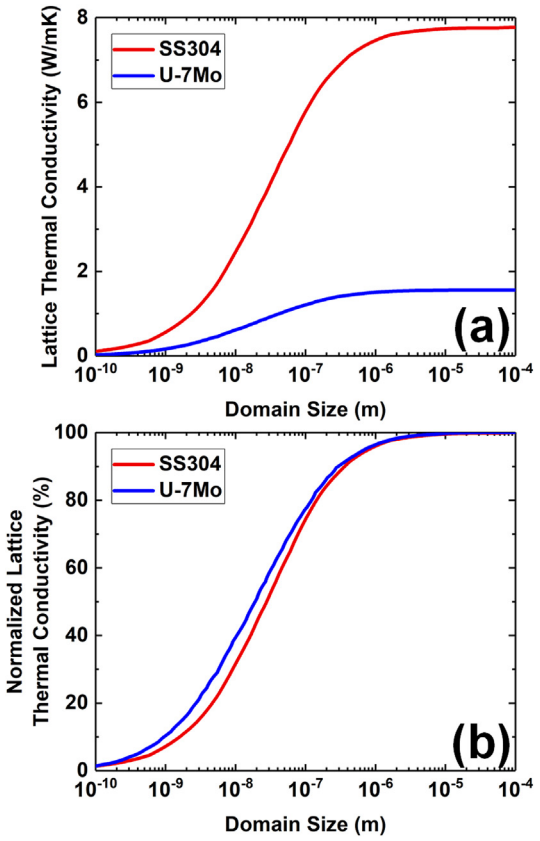

Fig. 7. Lattice thermal conductivity versus domain size in SS304 and U-Mo: (a) actual lattice thermal conductivity; (b) normalized lattice thermal conductivity.

conductivity of the atomized nominal U-7Mo particles seems to be close to the reported values for monolithic U-9Mo and U-10Mo, which are lower than the expected value for monolithic U-7Mo. According to the theoretical deduction discussed above, in alloy materials such as SS304 and U-Mo, the reduced specimen dimension (~300 nm) does not significantly affect the measured thermal conductivity values. Therefore, the minor difference between the measured value and expected value is expected to have other origins.

First, many of the literature data for U-Mo alloys were deduced from electrical conductivity based on the Wiedemann-Franz law, so that the accuracy of these data are affected by the selection of Lorentz number. The thermal conductivity of U-10Mo measured by laser flash method [29] is also slightly lower than other reported data. Second, the reported data of U-Mo are mainly from monolithic U-Mo alloys, while an atomized U-Mo particle was measured in this work. The difference in fabrication techniques may cause microstructural difference and, therefore, affect the thermal conductivity. Last but not least, the thermal conductivity of U-Mo is sensitive to the Mo content, which likely has local fluctuations. In this work, energy dispersive X-ray spectroscopy (EDS) was performed on the measured U-Mo specimens. The result shows an actual 8.2±0.4 wt% of Mo instead of the nominal U-7Mo composition. This may help explain the lower-than-expected measured thermal conductivity. Additionally, it is noticeable that the U-10Mo measurement [29] in Fig. 6(b) are also slightly lower than other reported data. These data were measured by the modern laser flash method and are expected to be more reliable than those data deduced from electrical conductivity. Thus, the slight difference observed in this study probably originates from the difference in

microstructure and the fluctuation in composition, instead of the size effect. Therefore, it is appropriate to apply the suspended bridge method to characterize the effects of radiation-induced microstructures on thermal conductivity in nuclear materials, especially alloy materials.

4.2. Insights for future applications

In this study, thermal conductivity of miniature specimens prepared by FIB were measured using a novel technique developed for nano-materials. The results are comparable with the reported values of bulk materials. It is shown that thermal conductivity data is barely affected by the size of the sample. This method is thus suitable for materials with low-mean-free-path carriers, such as alloys, which account for the majority of nuclear materials. After irradiation, the radiation damage further reduces the mean free path of both electrons and phonons, where this technique can be used to compare samples with a range of microstructures. By reducing the specimen dimension, the microstructures induced by either in-pile neutron irradiation or heavy ion irradiation can be separated from the bulk nuclear materials and then independently measured. We anticipate that this will elucidate questions that have persisted in the nuclear material community for decades, such as the thermal conductivity of interaction layers in U-Mo dispersion fuel, and the single phases of metallic fast reactor fuels (U-10Zr and U-xPu-10Zr). Additionally, as thermal conductivity of UO_2 below 1400 K is mainly contributed by phonons with a mean free path of few nm [42], the thermal conductivity of irradiated UO_2, especially the high-burnup structure (HBS), may also be investigated using the method developed in this study. The knowledge about the thermal conductivity of these radiation-induced microstructures can help improve the reliability and accuracy of advanced modeling and simulations of nuclear materials performance.

5. Conclusions

In this study, a novel thermal conductivity measurement technique developed for nanomaterials was applied to miniature specimens separated from bulk stainless steels and U-Mo alloy. The measurement results demonstrate that this technique yields thermal conductivity values that are comparable to bulk materials. Theoretical analyses of the results indicate that the method is capable of providing thermal conductivity measurements for materials with major carrier mean free paths that are significantly lower than the specimen dimension. The successful implementation of this nano-technique to nuclear material research will shed light upon the development of advanced modeling and simulation tools for nuclear materials.

Data availability statement

The raw/processed data required to reproduce these findings cannot be shared at this time as the data also forms part of an ongoing study.

Acknowledgments

This work was sponsored by the U.S. Department of Energy, Office of Material Management and Minimization in the U.S. National Nuclear Security Administration Office of Defense Nuclear Nonproliferation under Contract DE-AC02-06CH11357. S.S. acknowledges support from the National Science Foundation under Grant NSF-CBET-17-06854. The authors would like to thank KAERI for manufacturing and providing the U–Mo particles.

Appendix A. Supplementary data

Supplementary data to this article can be found online at https://doi.org/10.1016/j.jnucmat.2019.151797.

References

[1] S.J. Zinkle, G. Was, Acta Mater. 61 (2013) 735–758.
[2] K.A. Terrani, D. Wang, L.J. Ott, R.O. Montgomery, J. Nucl. Mater. 448 (2014) 512–519.
[3] A. Aitkaliyeva, L. He, H. Wen, B. Miller, X.-M. Bai, T. Allen, Structural Materials for Generation IV Nuclear Reactors, Elsevier, 2017, pp. 253–283.
[4] J.J. Powers, B.D. Wirth, J. Nucl. Mater. 405 (2010) 74–82.
[5] J. Gan, D.D. Keiser Jr., D.M. Wachs, A.B. Robinson, B.D. Miller, T.R. Allen, J. Nucl. Mater. 396 (2010) 234–239.
[6] S. Van den Berghe, W. Van Renterghem, A. Leenaers, J. Nucl. Mater. 375 (2008) 340–346.
[7] Y. Miao, K. Mo, B. Ye, L. Jamison, Z.-G. Mei, J. Gan, B. Miller, J. Madden, J.-S. Park, J. Almer, et al., Scr. Mater. 114 (2016) 146–150.
[8] B. Ye, L. Jamison, Y. Miao, S. Bhattacharya, G. Hofman, A. Yacout, J. Nucl. Mater. 488 (2017) 134–142.
[9] L. Tan, X. Ren, K. Sridharan, T. Allen, Corros. Sci. 50 (2008) 3056–3062.
[10] T. Baba, A. Ono, Meas. Sci. Technol. 12 (2001) 2046.
[11] Z. Hua, H. Ban, M. Khafizov, R. Schley, R. Kennedy, D.H. Hurley, J. Appl. Phys. 111 (2012) 103505.
[12] M. Khafizov, I.-W. Park, A. Chernatynskiy, L. He, J. Lin, J.J. Moore, D. Swank, T. Lillo, S.R. Phillpot, A. El-Azab, et al., J. Am. Ceram. Soc. 97 (2014) 562–569.
[13] D.H. Hurley, R.S. Schley, M. Khafizov, B.L. Wendt, Rev. Sci. Instrum. 86 (2015) 123901.
[14] P. Kim, L. Shi, A. Majumdar, P.L. McEuen, Phys. Rev. Lett. 87 (2001) 215502.
[15] L. Shi, D. Li, C. Yu, W. Jang, D. Kim, Z. Yao, P. Kim, A. Majumdar, J. Heat Transf. 125 (2003) 881–888.
[16] D. Li, Y. Wu, P. Kim, L. Shi, P. Yang, A. Majumdar, Appl. Phys. Lett. 83 (2003) 2934–2936.
[17] L. Shi, Q. Hao, C. Yu, N. Mingo, X. Kong, Z. L. Wang, in: ASME 2004 Heat Transfer/Fluids Engineering Summer Conference, American Society of Mechanical Engineers, pp. 457–461.
[18] M. Ghossoub, K. Valavala, M. Seong, B. Azeredo, K. Hsu, J. Sadhu, P. Singh, S. Sinha, Nano Lett. 13 (2013) 1564–1571.
[19] X. Iltis, I. Zacharie-Aubrun, H.J. Ryu, J. Park, A. Leenaers, A. Yacout, D. Keiser, F. Vanni, B. Stepnik, T. Blay, et al., J. Nucl. Mater. 495 (2017) 249–266.
[20] K.C. Mills, Y. Su, Z. Li, R.F. Brooks, ISIJ Int. 44 (2004) 1661–1668.
[21] R. Bogaard, P. Desai, H. Li, C. Ho, Thermochim. Acta 218 (1993) 373–393.
[22] J. Sweet, E. Roth, M. Moss, Int. J. Thermophys. 8 (1987) 593–606.
[23] Progress Report on Metallurgy of TubaClloy to University of Chicago from Battelle Memorial Institute, Battelle Memorial Institute, Columbus, OH, 1945. Technical Report CT-2632.
[24] R. Westphal, Thermal Conductivity of Reactor Fuel Element Materials, Westinghouse Electric Corp. Atomic Power Div., Pittsburgh, 1954. Technical Report.
[25] R. Hengstler, L. Beck, H. Breitkreutz, C. Jarousse, R. Jungwirth, W. Petry, W. Schmid, J. Schneider, N. Wieschalla, J. Nucl. Mater. 402 (2010) 74–80.
[26] S. Konobeevsky, A. Zaimovsky, B. Levitsky, Y. Sokursky, N. Chebotarev, Y. V. Bobkov, P. Egorov, G. Nikolaev, A. Ivanov, in: Proc. Second United Nations International Conference on the Peaceful Uses of Atomic Energy, Volume 6, United Nations Geneva, pp. 194–203.
[27] T. Matsui, T. Natsume, K. Naito, J. Nucl. Mater. 167 (1989) 152–159.
[28] J. Klein, Uranium and its Alloys, Wiley, New York-London, 1962.
[29] S. Lee, J. Kim, J. Park, H. Ryu, C. Kim, in: Proceedings of the RERTR Meeting, Las Vegas, Nevada.
[30] C. Roy, A. Radenac, F. Cado, J. Nucl. Mater. 48 (1973) 369–371.
[31] H.A. Saller, R. Dickerson, A. Bauer, N. Daniel, Properties of a Fissium-type Alloy, Battelle Memorial Inst., Columbus, Ohio, 1956. Technical Report.
[32] D.E. Burkes, C.A. Papesch, A.P. Maddison, T. Hartmann, F.J. Rice, J. Nucl. Mater. 403 (2010) 160–166.
[33] D. Gall, J. Appl. Phys. 119 (2016) 085101.
[34] O. Hellman, I.A. Abrikosov, Phys. Rev. B 88 (2013) 144301.
[35] O. Hellman, D.A. Broido, Phys. Rev. B 90 (2014) 134309.
[36] O. Hellman, I. Abrikosov, S. Simak, Phys. Rev. B 84 (2011) 180301.
[37] O. Hellman, P. Steneteg, I.A. Abrikosov, S.I. Simak, Phys. Rev. B 87 (2013) 104111.
[38] P.E. Blöchl, Phys. Rev. B 50 (1994) 17953.
[39] G. Kresse, et al., Phys. Rev. B 54 (1996) 11169.
[40] G. Kresse, Phys. Rev. B 59 (1999) 1758.
[41] J.P. Perdew, Phys. Rev. Lett. 77 (1996) 3865.
[42] J. Moore, D. McElroy, J. Am. Ceram. Soc. 54 (1971) 40–46.